Efficiency enhancement of silicon solar cells using a nano-scale honeycomb broadband anti-reflection structure

C.K. Huang,[1] K.W. Sun,[1,*] and W.-L. Chang[2]

[1] *Department of Applied Chemistry, National Chiao Tung University, Hsinchu, Taiwan*
[2] *Green Energy & Environment Research Laboratories (GEL), Industrial Technology Research Institute (ITRI), Hsinchu, Taiwan*
[*] *kwsun@mail.nctu.edu.tw*

Abstract: This experiment demonstrates the process for manufacturing a ZnO honeycomb sub-wavelength structure using nanosphere lithography technology exhibiting excellent anti-reflection properties from the UV to NIR wavelength regions. This honeycomb nanostructure, combined with commercially available crystalline Si solar cells, show substantially improved conversion efficiency from 15.6% to 16.6% using optimized honeycomb sizes and precursor concentrations of ZnO. The present work develops an unsophisticated and economical technique suitable for industrial applications in producing a uniform and low-reflective texture.

OCIS codes: (310.1210) Antireflection coatings; (310.6628) Subwavelength structures, nanostructures; (040.5350) Photovoltaic.

References and links

1. W. Joo, H. J. Kim, and J. K. Kim, "Broadband antireflection coating covering from visible to near infrared wavelengths by using multilayered nanoporous block copolymer films," Langmuir **26**(7), 5110–5114 (2010).
2. J. Li, H. Yu, S. M. Wong, G. Zhang, X. Sun, P. G.-Q. Lo, and D.-L. Kwong, "Si nanopillar array optimization on Si thin films for solar energy harvesting," Appl. Phys. Lett. **95**(3), 033102 (2009).
3. H. Zhou, T. Fan, T. Han, X. Li, J. Ding, D. Zhang, Q. Guo, and H. Ogawa, "Bacteria-based controlled assembly of metal chalcogenide hollow nanostructures with enhanced light-harvesting and photocatalytic properties," Nanotechnology **20**(8), 085603 (2009).
4. K.-S. Han, J.-H. Shin, W.-Y. Yoon, and H. Lee, "Enhanced performance of solar cells with anti-reflection layer fabricated by nano-imprint lithography," Sol. Energy Mater. Sol. Cells **95**(1), 288–291 (2011).
5. Y. Li, J. Zhang, and B. Yang, "Antireflective surfaces based on biomimetic nanopillared arrays," Nano Today **5**(2), 117–127 (2010).
6. J. Y. Chen and K. W. Sun, "Enhancement of the light conversion efficiency of silicon solar cells by using nanoimprint anti-reflection layer," Sol. Energy Mater. Sol. Cells **94**(3), 629–633 (2010).
7. S. Chattopadhyay, Y. F. Huang, Y. J. Jen, A. Ganguly, K. H. Chen, and L. C. Chen, "Anti-reflecting and photonic nanostructures," Mater. Sci. Eng. Rep. **69**(1-3), 1–35 (2010).
8. Y.-F. Huang, S. Chattopadhyay, Y.-J. Jen, C.-Y. Peng, T.-A. Liu, Y.-K. Hsu, C.-L. Pan, H.-C. Lo, C.-H. Hsu, Y.-H. Chang, C.-S. Lee, K.-H. Chen, and L.-C. Chen, "Improved broadband and quasi-omnidirectional anti-reflection properties with biomimetic silicon nanostructures," Nat. Nanotechnol. **2**(12), 770–774 (2007).
9. J. Y. Chen, W. L. Chang, C. K. Huang, and K. W. Sun, "Biomimetic nanostructured antireflection coating and its application on crystalline silicon solar cells," Opt. Express **19**(15), 14411–14419 (2011).
10. M. Y. Chiu, C. H. Chang, M. A. Tsai, F. Y. Chang, and P. C. Yu, "Improved optical transmission and current matching of a triple-junction solar cell utilizing sub-wavelength structures," Opt. Express **18**(S3 Suppl 3), A308–A313 (2010).
11. C. K. Huang, H. H. Lin, J. Y. Chen, K. W. Sun, and W. L. Chang, "Efficiency enhancement of the poly-silicon solar cell using self-assembled dielectric nanoparticles," Sol. Energy Mater. Sol. Cells **95**(8), 2540–2544 (2011).
12. J. Zhao, A. Wang, P. Altermatt, and M. A. Green, "Twenty-four percent efficient silicon solar cells with double layer antireflection coatings and reduced resistance loss," Appl. Phys. Lett. **66**(26), 3636 (1995).
13. J. H. Zhao, A. H. Wang, M. A. Green, and F. Ferrazza, "19.8% efficient "honeycomb" textured multicrystalline and 24.4% monocrystalline silicon solar cells," Appl. Phys. Lett. **73**(14), 1991–1993 (1998).
14. H. Morikawa, D. Niinobe, K. Nishimura, S. Matsuno, and S. Arimoto, "Processes for over 18.5% high-efficiency multi-crystalline silicon solar cell," Curr. Appl. Phys. **10**(2), S210–S214 (2010).
15. A. Parretta, A. Sarno, P. Tortora, H. Yakubu, P. Maddalena, J. H. Zhao, and A. H. Wang, "Angle-dependent reflectance measurements on photovoltaic materials and solar cells," Opt. Commun. **172**(1-6), 139–151 (1999).

#156802 - $15.00 USD Received 19 Oct 2011; revised 24 Nov 2011; accepted 8 Dec 2011; published 20 Dec 2011

16. E. Manea, E. Budianu, M. Purica, C. Podaru, A. Popescu, I. Cernica, F. Babarada, and C. C. Parvulescu, "SnO2 thin films prepared by sol gel method for 'Honeycomb' textured silicon solar cells," Rom. J. Inform. Sci. Technol **10**, 25–33 (2007).
17. X.-T. Zhang, O. Sato, M. Taguchi, Y. Einaga, T. Murakami, and A. Fujishima, "Self-cleaning particle coating with antireflection properties," Chem. Mater. **17**(3), 696–700 (2005).
18. S. Walheim, E. Schaffer, J. Mlynek, and U. Steiner, "Nanophase-separated polymer films as high-performance antireflection coatings," Science **283**(5401), 520–522 (1999).
19. B. Kim, J. Bang, S. Jang, D. Kim, and J. Kim, "Surface texturing of GaAs using a nanosphere lithography technique for solar cell applications," Thin Solid Films **518**(22), 6583–6586 (2010).
20. D. Derkacs, S. H. Lim, P. Matheu, W. Mar, and E. T. Yu, "Improved performance of amorphous silicon solar cells via scattering from surface plasmon polaritons in nearby metallic nanoparticles," Appl. Phys. Lett. **89**(9), 093103 (2006).
21. D. M. Schaadt, B. Feng, and E. T. Yu, "Enhanced semiconductor optical absorption via surface plasmon excitation in metal nanoparticles," Appl. Phys. Lett. **86**(6), 063106 (2005).
22. S. H. Lim, W. Mar, P. Matheu, D. Derkacs, and E. T. Yu, "Photocurrent spectroscopy of optical absorption enhancement in silicon photodiodes via scattering from surface plasmon polaritons in gold nanoparticles," J. Appl. Phys. **101**(10), 104309 (2007).
23. S. Pillai, K. R. Catchpole, T. Trupke, and M. A. Green, "Surface plasmon enhanced silicon solar cells," J. Appl. Phys. **101**(9), 093105 (2007).
24. H. R. Stuart and D. G. Hall, "Absorption enhancement in silicon-on-insulator waveguides using metal island films," Appl. Phys. Lett. **69**(16), 2327–2329 (1996).
25. Y. Lalatonne, J. Richardi, and M. P. Pileni, "Van der Waals versus dipolar forces controlling mesoscopic organizations of magnetic nanocrystals," Nat. Mater. **3**(2), 121–125 (2004).
26. K. A. Alim, V. A. Fonoberov, M. Shamsa, and A. A. Balandin, "Micro-Raman investigation of optical phonons in ZnO nanocrystals," J. Appl. Phys. **97**(12), 124313 (2005).
27. D. Li, Y. H. Leung, A. B. Djurišić, Z. T. Liu, M. H. Xie, S. L. Shi, S. J. Xu, and W. K. Chan, "Different origins of visible luminescence in ZnO nanostructures fabricated by the chemical and evaporation methods," Appl. Phys. Lett. **85**(9), 1601–1603 (2004).
28. L. E. Greene, M. Law, J. Goldberger, F. Kim, J. C. Johnson, Y. Zhang, R. J. Saykally, and P. Yang, "Low-temperature wafer-scale production of ZnO nanowire arrays," Angew. Chem. Int. Ed. Engl. **42**(26), 3031–3034 (2003).
29. Structural Colors in Biological Systems, *Principles and Applications,* eds. S. Kinoshita and S. Yoshioka (Osaka University Press, 2005).
30. P. B. Clapham and M. C. Hutley, "Reduction of lens reflexion by the 'Moth Eye' principle," Nature **244**(5414), 281–282 (1973).
31. Y. Zhao, X. T. Zhang, J. Zhai, J. L. He, L. Jiang, Z. Y. Liu, S. Nishimoto, T. Murakami, A. Fujishima, and D. B. Zhu, "Enhanced photocatalytic activity of hierarchically micro-/nano-porous TiO2 films," Appl. Catal. B **83**(1-2), 24–29 (2008).

1. Introduction

To fabricate solar cells with high conversion efficiency, the reduction of reflectivity at the surface of solar cells is very important. Anti-reflection (AR) layers with ordered micro/nanostructured arrays of uniform shapes and sizes have attracted growing interest recently because of their applications in light harvesting [1–11]. The inverted pyramid surface texturing has been experimentally proven to be very effective in trapping light by total internal reflection. An increase of the solar cell's effective optical thickness by a factor as high as 40 has been demonstrated [12]. However, such surface texturing relies on anisotropic etching to expose intersecting {111} crystal planes forming pyramid sides, making this approach unsuitable for multi-crystalline (mc-Si) substrates.

Honeycomb texturing has recently been demonstrated to improve both the transmission of photons into active layers of the semiconductors and the coupling of normally incident photons into the lateral, optically confined paths within the P-N junction layer, resulting in the increased photon absorption, photo-current generation, and power conversion efficiency of the cell [13–15]. This structure gives the maximum well packing density, reducing surface re⟩ection through the so-called double bounce effect. Cells with a honeycomb structure of hemispherical wells have shown a slightly higher reflection with respect to the passivated emitter, rear locally diffused cells, particularly at the highest angles of incidence, but a better transmittance relative to the normal incidence up to 60° in the 500 nm to 600 nm wavelength range [15]. An improved efficiency of 19.8% for a mc-Si solar cell with an incorporated hexagonally symmetrical "honeycomb" surface texture was reported [13]. More recently, a novel honeycomb texturization method by combining laser patterning and wet chemical

#156802 - $15.00 USD Received 19 Oct 2011; revised 24 Nov 2011; accepted 8 Dec 2011; published 20 Dec 2011

etching has achieved 18.6% efficiency in mc-Si solar cells with a micrometer-scale hexagonal pattern [14].

The size of the hemispherical wells in the honeycomb structure used in previous studies is typically approximately 14μm to 20μm [14–16]. However, the chemical wet etching method used to generate the honeycomb structure is incapable of precisely controlling the size of hemispherical wells and substrate material. The lithography process is also complicated and is not applicable to large-scale and high throughput industrial production.

On the other hand, nanoporous AR surfaces with domain sizes smaller than the wavelength of light have been demonstrated as an effective AR coating with tunable effective refractive indices [17, 18]. A nanoporous film with a refractive index as low as 1.14 was prepared from a polystyrene-poly (methyl methacylate) diblock coplymer mixture, which showed a broadband AR coating with a transmission of 99.7% [18]. A single layer submicrometer-sized SiO_2 particle was used to provide a porous structure with low refractive index, which induces the AR effect [17]. Nevertheless, nanoporous AR films have never been successfully demonstrated on practical solar cells.

By combining the honeycomb effect (or double bounce effect) with nanopore surface characteristics (high surface areas and low average refractive indices), substantial enhancement on cell efficiency is expected with the integration of the nano-scale honeycomb AR coating. The present work demonstrates a self-assembled nanoparticle lift-off technique [11, 19–24] that can uniformly cover the surface of conventional crystalline Si (c-Si) solar cells with a nano-scale honeycomb structured layer (NHSL) of zinc oxide (ZnO) to achieve the goal of manufacturing the abovementioned AR coating in a high-speed, inexpensive, and reproducible manner. Most importantly, this technique is not limited by the substrate materials. The current research also investigates the performance of c-Si solar cells incorporated with the NHSL using dielectric polystyrene (PS) nanospheres with particle sizes ranging from 100 nm to 500 nm. The coexistence of the nano/micro scale surface texture on the commercial c-Si cells is proved to enhance the cell efficiency and light harvesting capability further.

2. Experiment process

The c-Si solar cell used in the present study was prepared by the following commercial fabrication processes. The p-type Si wafers were roughened using potassium hydroxide (KOH), resulting in damage etch with no additional texturization. A 500 nm n-type layer was created on the texture by $POCl_3$ diffusion using a centrotherm tube furnace to form the p-n junction, followed by the depositing of a thin anti-reflection layer of 80 nm SiNx using a centrotherm direct plasma-enhanced chemical vapor deposition furnace. The front- and rear-side finger and bus bar contacts were screen-printed using standard, commercially available lead containing Ag, Al, and Ag+Al pastes using a semi-automatic ATMASC 25PP printer. The cells were fired using a fast firing conveyor belt furnace at an optimal firing temperature of 850 °C to facilitate contact between the fingers, bus bars, the N- and P-type regions for maximum performance. Finally, the cell edges were isolated using a 532 nm Nd:YAG laser cutting tool.

PS nanoparticles (purchased from the Golden Innovation Corp.) with diameters of 100, 250, and 500 nm were first dispersed in a surfactant (mixture of MA/X-100 with a ratio of 400:1 by weight) to yield a 2.5 wt % suspension solution. Large-area colloidal crystal multilayers (over 7.0 cm^2) were formed on the cell surface by a self-assembly process because of the van der Waals force [25] with a custom-built spin coater. $Zn(Ch_3COOH)_2$ solutions with different concentrations were prepared from $Zn(Ch_3COOH)_2•2H_2O$) dissolved in distilled water.

The PS colloidal crystal multilayers were first deposited on the solar cell surface as a mask for the subsequent lift-off process. A drop (approximately 300μl) of the $Zn(Ch_3COOH)_2$ solution was dripped on the 3D colloidal crystal multilayers using a quantitative pipette. The solution was able to in□ltrate into the interstices between the cell surface and PS colloidal multilayers. The sample was then placed into an oven and dried at 85 °C for 2 hours, followed

#156802 - $15.00 USD Received 19 Oct 2011; revised 24 Nov 2011; accepted 8 Dec 2011; published 20 Dec 2011

by heating at 300 °C for 1 hour to burn off the latex spheres and decompose the $Zn(Ch_3COOH)_2$ into ZnO. The burning temperature was kept adequately low so that the Si p-n junction underneath will not be affected. Figure 1 shows a schematic diagram of the formation of ZnO NHSL on the micro-textured cell surface.

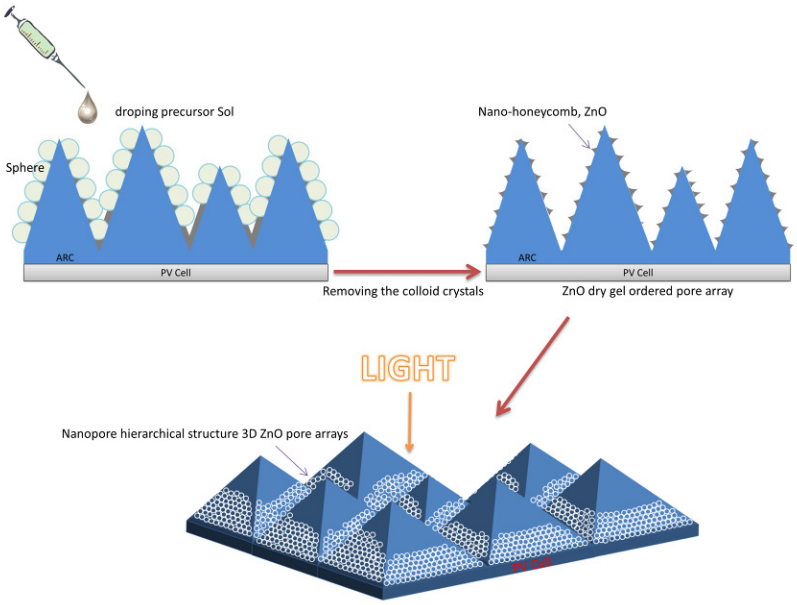

Fig. 1. Schematics of the fabrication processes for the 3D nano-scale honeycomb structures on micro-scale texture.

The NHSL was patterned on top of the commercially processed c-Si solar cells with a light absorption area of 1.5 cm × 1.5 cm. All solar cell devices with and without the NHSL were evaluated at room temperature based on the illuminated current density versus voltage (J-V) characteristics, the external quantum efficiency (EQE), and the reflectance. The photocurrent was analyzed using a solar simulator under the Air Mass 1.5 Global (AM 1.5 G) illumination condition (100 mW/cm^2, 25 °C). The EQE was measured using an AM 1.5 G standard spectrum and an Optosolar simulator (SR-150). The reflectance spectra of the samples were recorded using a UV-Visible-NIR spectrophotometer (Hitachi U-4100) for wavelengths ranging from 200 nm to 1200 nm. X-ray diffraction (XRD) and the energy disperse spectrum of X-rays (EDS) of the samples were measured on a Bruker AXS D8 advanced automatic diffractometer with Cu Kα radiation and Oxford INCA Energy 350, respectively. The Raman signals from the samples were collected through a confocal microscope and analyzed using a spectrometer equipped with a liquid nitrogen (LN)-cooled charge-coupled device detector at the excitation wavelength of 488 nm.

3. Results and discussion

In Fig. 2, the scanning electron microscope (SEM) image shows that the as prepared ZnO NHSL AR film (using the 250 nm PS nanoparticle as the hard mask) contains ordered 3D structures of nano-scale honeycombs with a thickness of 2 to 3 layers on the c-Si cell surface. The enlarged SEM image in the inset of Fig. 2 clearly shows that the NHSL displays a hexagonal close-packed alignment with a periodicity of 250 nm and approximately a hollow hemispherical shape with a diameter of 240 nm.

#156802 - $15.00 USD Received 19 Oct 2011; revised 24 Nov 2011; accepted 8 Dec 2011; published 20 Dec 2011

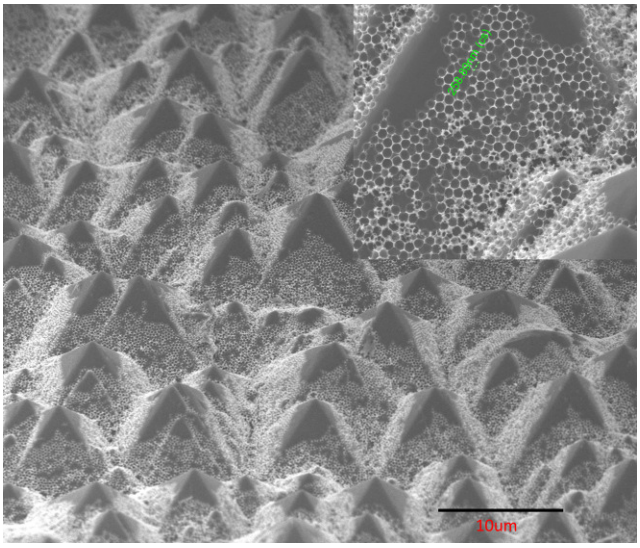

Fig. 2. SEM image of the NHSL on the textured solar cell surface. The inset shows the enlarged image.

Figure 3 displays the nonresonant Raman spectrum of the NHSL. The peaks at 436 cm^{-1} and 576 cm^{-1} are attributed to the E_2(high), and A_1(LO) phonons, respectively. The peak at approximately 330 cm^{-1} is attributed to the second-order Raman processes [26]. No TO phonons were observed in the Raman spectrum, indicating that the characteristics of the NHSL are similar to the ZnO nanocrystals reported in Ref [26]. From the analysis of the EDS, as shown in Fig. 4, the NHSL is found to be made of ZnO. However, the XRD pattern shown in the inset of Fig. 4 displays no diffraction peaks, further confirming that the NHSL is unlikely to be in the crystalline phase because of the low growth temperature at 300 °C.

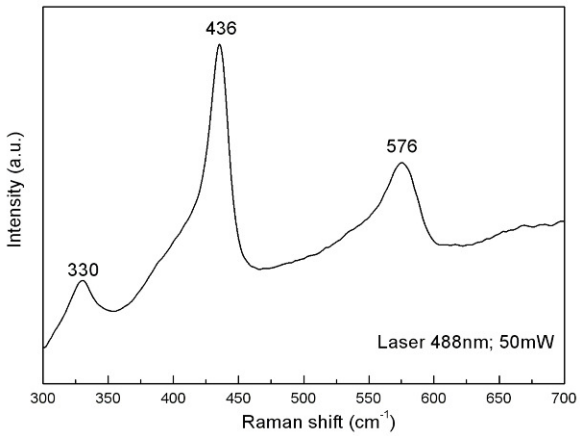

Fig. 3. Nonresonant Raman spectrum of NHSL excited with a laser at 488 nm and a power of 50 mW.

#156802 - $15.00 USD Received 19 Oct 2011; revised 24 Nov 2011; accepted 8 Dec 2011; published 20 Dec 2011

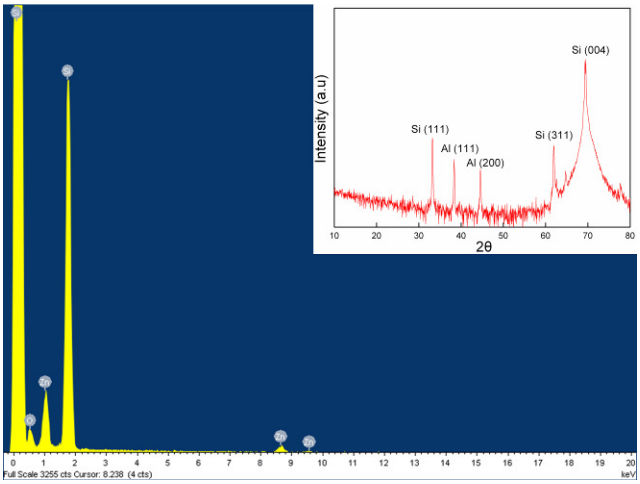

Fig. 4. The EDS results of ZnO NHSL. The inset gives the XRD pattern.

Absorption and photoluminescence spectra (not shown) were also measured from the ZnO NHSL reproduced on a transparent substrate. The NHSL only shows an insignificant UV absorption near the ZnO band edge. A very weak yellow emission centered at 579 nm attributed to the presence of oxygen interstitials is also found in the PL spectra, which is a common feature in samples is prepared using simple chemical methods [27, 28]. The overall light transmission through the transparent substrate is enhanced with the presence of the NHSL.

To determine the best combination, NHSL with PS particle sizes of 100, 250, and 500 nm and different precursor concentrations of $Zn(Ch_3COOH)_2$ (i.e., 0.05, 0.1, 0.15, 0.2 and 0.3 M, respectively) was used in the experiment at a fixed spin rate and dose. Figures 5 (a)-(c) show the reflectance of the NHSL with different particle sizes and precursor concentrations at a fixed spin rate and dose volume. The reflectance spectrum of cells without NHSL is also displayed in parallel for comparison. The reason for reduction in the reflectance shown in Fig. 5 is twofold. First, in the visible and IR regions, the effective refractive index is low because of the sub-wavelength nanoporous structures of the NSHL [18]. Second, for the UV light, the nano-scale honeycombs allow the multiple scattering of photons through the film, thus increasing the optical path [12–14].

The optimized precursor concentrations for 100, 250, and 500 nm particle sizes were 0.05, 0.1 and 0.15 M, respectively, before the surface turns semi-opaque. Figure 6 shows the corresponding FESEM images of the NHSL. The images show that the average pore diameters on the NHSL are 90, 240 and 490 nm for the 100, 250, and 500 nm PS nanoparticles at the precursor concentrations of 0.05, 0.1, and 0.15 M, respectively. Figure 7 shows the maximum enhancement of the absorbed power in the c-Si solar cells with the NHSL obtained after the optimization of the PS nanoparticle sizes and precursor concentrations. The best overall power conversion efficiency, η, increases from 15.6% to 16.6%. The increase in the conversion efficiency of the solar cells with the NHSL are 1.0%, 0.7%, and 0.4% for the 100, 250, and 500 nm PS nanoparticle sizes, respectively.

The highest efficiency increase of 1.0% was achieved when the solar cell surface was coated with the NHSL AR layer with a 90 nm pore diameter. However, the enhancement factors began to drop when the pore sizes on the NHSL increased. This phenomenon is attributed to the reduction in porosity (or surface to volume ratio) as the diameters of pores are increased [18]. The proposed NHSL, which acts similar to “nanopore thin film”, has the following advantages over the conventional AR thin films. First, the hierarchically structured NHSL has a higher surface-to-volume ratio, facilitating the scattering of photons into the porous structure. The second advantage is that the structure is also strongly light scattering,

#156802 - $15.00 USD Received 19 Oct 2011; revised 24 Nov 2011; accepted 8 Dec 2011; published 20 Dec 2011

resulting in multiple passes of photons through the film, thus increasing the light absorption [29–31].

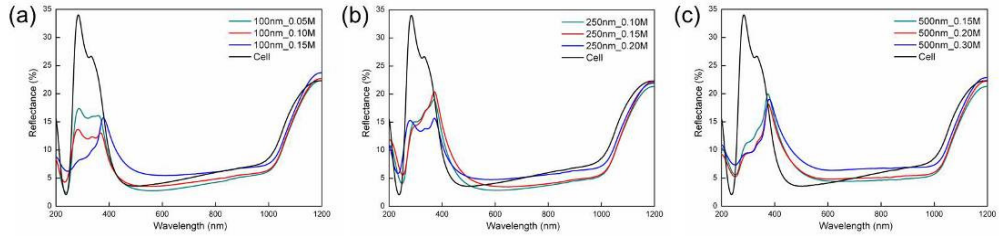

Fig. 5. Reflectance spectra at maximum performance of solar cells integrated with NHSL with PS nanoparticle sizes of (a) 100 nm, (b) 250 nm and (c) 500 nm at different precursor concentrations of ZnO. The spectrum of an untreated device is also presented in parallel for comparison.

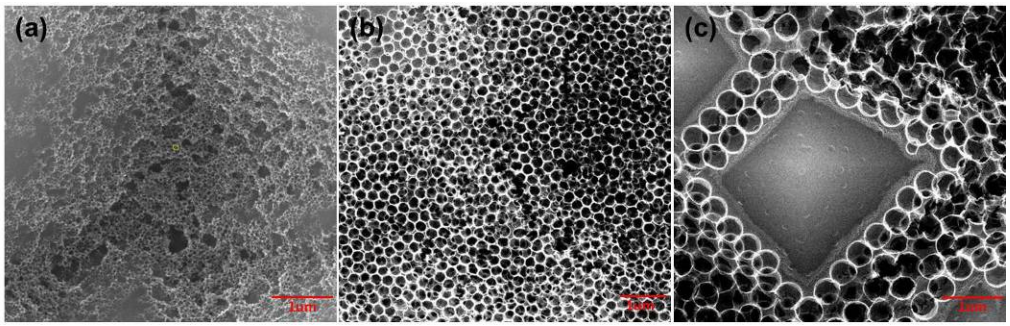

Fig. 6. FESEM images of ZnO NHSL on c-Si solar cell prepared with PS nanoparticles with sizes of (a) 100 nm, (b) 250 nm, and (c) 500 nm.

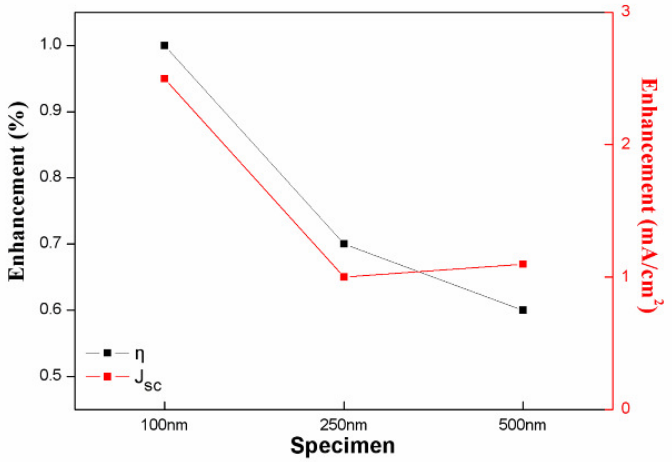

Fig. 7. Gains in conversion efficiency and current density of c-Si solar cells after optimization of NHSL pore sizes and precursor concentrations of ZnO.

Figure 8 shows the current-voltage (J-V) characteristic of the solar cell at maximum enhancement. The performance of the cell without the NHSL is also presented in parallel for comparison. The short-circuit current density (J_{SC}), open-circuit voltage (V_{OC}), fill factor (FF), and conversion efficiency for the experiment cells are 43.5 mA/cm^2, 0.56 V, 0.68, and 16.6%, respectively, and for the reference cells, the values are 41.0 mA/cm^2, 0.56 V, 0.67, and 15.6%, respectively. V_{OC} and FF remain almost unaffected as the J_{SC} increases from 41.0 to 43.5

#156802 - $15.00 USD Received 19 Oct 2011; revised 24 Nov 2011; accepted 8 Dec 2011; published 20 Dec 2011

mA/cm^2 with the NHSL on the textured surface. Therefore, the enhancement of cell efficiency is indeed attributable to the increase in photocurrent and light absorption.

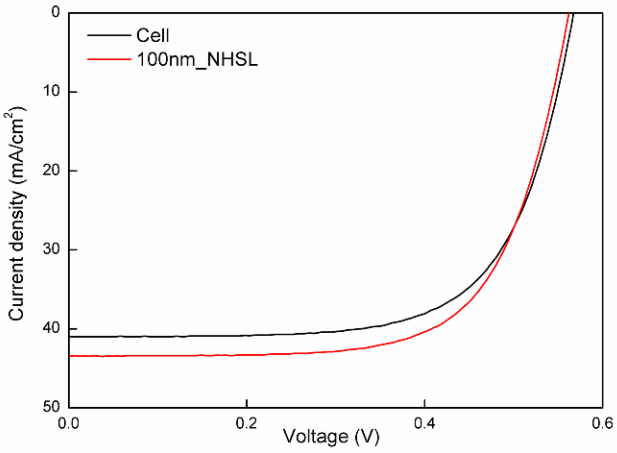

Fig. 8. J-V characteristics of the optimized solar cells integrated with the NHSL in compared to devices without the NHSL.

The EQE of the c-Si solar cells coated with NHSL of different pore sizes are measured and compared with the cells without NHSL. Figure 9 shows the results. The increase in photocurrent clearly results from the enhanced absorption of light by the active layer. The EQE measurements are in agreement with the reflectance results wherein light harvesting is improved in the wavelength ranges of 400 and 1100 nm because of the presence of NHSL. The EQE achieves over 95% within a broad wavelength range from 400 nm to 800 nm, showing a signi□cant improvement over conventional cells.

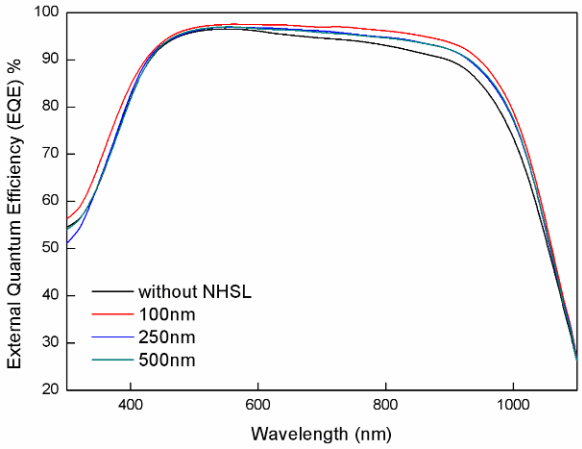

Fig. 9. External quantum efficiency at maximum performance measured under AM 1.5 G illumination for solar cells integrated with NHSL for PS nanoparticle sizes of 100, 250, 500 nm. Results from an untreated device is also displayed in parallel for comparison.

4. Conclusion

In conclusion, a viable solution to enhance light harvesting by applying nano-scale honeycomb structures on a commercial c-Si solar cell was demonstrated. Cells integrated with the NHSL were found to achieve over 95% external quantum efficiencies within a broad wavelength range from 400 nm to 800 nm and an efficiency increase of 1.0%. The manufacture of such cells is inexpensive and reproducible, without the need for specialized

#156802 - $15.00 USD Received 19 Oct 2011; revised 24 Nov 2011; accepted 8 Dec 2011; published 20 Dec 2011

equipments. The process would be suitable for industrial applications with respect to the lithography process utilized for producing a uniform, low-reflective texture on Si wafers.

Acknowledgments

The present work was partially supported by the Bureau of Energy in Taiwan and National Science Council of the Republic of China under Grant No. NSC 99-2119-M-009-004-MY3.

#156802 - $15.00 USD Received 19 Oct 2011; revised 24 Nov 2011; accepted 8 Dec 2011; published 20 Dec 2011